Slippery Liquid-Infused Porous Surfaces (SLIPS) and Surface Acoustic Wave Droplet Transportation

J. T. Luo[1,2], N. R. Geraldi[2], J. H. Guan[2], G. McHale[2], G. G . Wells[2], Y. Q. Fu[2*]

[1]College of Physics and Energy, Shenzhen Key Laboratory of Sensor Technology, Shenzhen University, Shenzhen, 518060, People's Republic of China

[2]Smart Materials and Surfaces Laboratory, Faculty of Engineering and Environment, Northumbria University, Newcastle upon Tyne, NE1 8ST, UK

*corresponding author: Dr. Richard Y. Q. Fu, email: richard.fu@northumbria.ac.uk

ABSTRACT

On a solid surface a droplet of liquid will stick due to the capillary adhesion and this causes low droplet mobility. To reduce contact line pinning, surface chemistry can be coupled to micro- and/or nano-structures to create superhydrophobic surfaces on which a droplet balls-up into an almost spherical shape thus minimising contact area. Recent progress in soft matter has now led to alternative lubricant impregnated surfaces capable of almost zero contact line pinning and high droplet mobility without causing droplets to ball-up and minimize contact area. Here we report a new approach to Surface Acoustic Wave (SAW) actuated droplet transportation enabled using such a surface. These surfaces maintain the contact area required for efficient energy and momentum transfer of the wave energy into the droplet, whilst achieving high droplet mobility and large footprint, therefore reducing the threshold power required to induce droplet motion. In our approach we used a slippery layer of lubricating oil infused into a self-assembled porous hydrophobic layer, which is significantly thinner than the SAW wavelength and so avoided damping of the wave. A significant reduction (up to 85%) in the threshold power for droplet transportation was found compared to that using a conventional surface treatment method. Moreover, unlike droplets on superhydrophobic surfaces, where interaction with the SAW induced a transition from a Cassie–Baxter state to a Wenzel state, the droplets on our liquid impregnated surfaces remained in a mobile state after interaction with the SAW.

Keywords: Surface acoustic wave (SAW), SLIPS, droplet transportation, superhydrophobic.

I. INTRODUCTION

A fundamental problem in any situation requiring mobility of liquid droplets is the contact line pinning caused by the inherent contact angle hysteresis, the difference between the advancing and receding contact angles, of liquids on solid surfaces [1-3]. Contact line pinning determines the formation of coffee ring-stains during the drying of droplets containing solute [4], which is an effect way that has to be carefully controlled in droplet microarrays [5] and inkjet printing [6]. It also causes barriers to droplet transport in microfluidics where a large surface area to volume ratio generally exists [7]. To minimize the effect of contact angle hysteresis on droplet mobility, the surface chemistry can be made hydrophobic, and by manipulating the surface topography superhydrophobic surfaces can be created [8-12]. A droplet in a Cassie-Baxter state (as shown in Fig.1 (a)) bridging between the tips of surface features on a superhydrophobic surface balls-up into an almost spherical shape. This minimizes the contact area and the effect of contact line pinning, thereby resulting in highly mobile droplets, unless the droplet transitions into a Wenzel state (see Fig.1 (b)) with liquid penetrating between the surface features [11].

1.1. Acoustofluidics

Recently, there has been increased interest in surface acoustic wave (SAW) based microfluidics (often called acoustofluidics) and biosensors due to their promising applications in the fields of lab-on-a-chip and point of care diagnosis [13-18]. For these applications, it is essential to develop strategies for reliable and efficient microfluidic functions and manipulation of particles and bio-molecules in the liquid,

such as in a droplet-digital microfluidics [19-21]. For such small volumes of liquid down to micro and nano litres, it is a challenge to efficiently manipulate and actuate droplets or liquid in microchannels due to the large surface area to volume ratio in microsystems and therefore the dominance of surface tension forces. This becomes particularly problematic with even modest levels of contact angle hysteresis, which results in contact line pinning [7, 22-24]. So far, various techniques have been employed to drive microscale fluids, including pressure gradients, capillary forces, electrical and magnetic fields, and SAWs [13, 19, 25]. SAW microfluidic actuation has significant advantages over other technologies, such as simple device structures, easy processing and low fabrication cost, tuneable frequency response, and the ability to manipulate liquids on a flat surface with precision [26].

For microfluidic applications Rayleigh SAWs, which propagate along a solid surface with their energy confined to within one wavelength of the surface, are often used [13, 15, 27, 28]. These are generated by applying a radio frequency (RF) signal to interdigital transducers (IDTs) which are patterned on top of a piezoelectric substrate (Fig. 2(a)). When the propagating SAWs contact with a droplet along its path, the leaky SAWs with decaying amplitudes are launched and dissipated into the droplet at an angle called the Rayleigh angle (θ_R) (see Fig. 2(b)), following Snell's law of diffraction [14]:

$$\theta_R = \sin^{-1}\left(\frac{c_l}{c_s}\right) \tag{1}$$

where c_l and c_s are the speeds of sound in the liquid and in the substrate, respectively. For SAW-induced droplet actuation on the substrate surface, coupling of the acoustic wave energy and transfer of momentum to the droplet is required. The energy and

momentum of the longitudinal wave dissipated into the droplet provide a pressure or a body force on the droplet in the direction of propagation of the SAW. This provides the basis for droplet movement, pumping and mixing, streaming, manipulation and jetting/nebulisation [13, 15, 26, 27, 29].

The piezoelectric materials used for SAW devices are mostly hydrophilic in nature (i.e., with low contact angles from 40^{o} to 60^{o}), and so to enhance the transportation of droplets on planar substrates, a hydrophobic treatment of the SAW device is often used. This reduces the length of the droplet-solid surface contact line, but also reduces the solid-liquid contact area critical to the acoustic wave-droplet interaction. Various hydrophobic polymer coatings, such as octadecyltrichlorosilane (OTS), Teflon AF® and CYTOP™ have previously been used to increase the contact angle of the droplet on the surface [13, 27-29]. Most of the hydrophobic polymers coated onto SAW device surfaces have contact angles of around 90-120° [13, 29-30]. Surfaces with such contact angles retain a sufficiently large footprint for the applied SAW power to be dissipated into the droplet through the wave/liquid interaction areas. However, the relatively large contact area when combined with the contact angle hysteresis, as described below, often results in a large power required to transport the droplet.

1.2. Contact Line Pinning and Superhydrophobicity

The SAW induced pressure gradient or a body force inside the droplet is dependent on the solid-liquid contact area and the input SAW power. A sufficient area is required for an effective acoustic wave-droplet interaction and thus the associated microfluidic functions. Increasing the input SAW power beyond a critical value causes the pressure gradient induced body force on the droplet to be larger than the pinning forces arising

from solid-liquid interfacial interactions, thus moving the droplet along the wave propagation direction.

For a small liquid droplet resting on a smooth solid surface, the force that must be overcome to create motion is related to the horizontal component of the solid-liquid surface tension force, $\gamma_{LG}\cos\theta$, where γ_{LG} is the liquid-gas interfacial tension, which is 72.8 mNm^{-1} for water in air at room temperature, and θ is the contact angle. On all solid surfaces some level of contact angle hysteresis is observed such that when the droplet volume is increased the initial effect is that the contact angle increases without motion of the contact line until an advancing contact angle, θ_A, is exceeded. Similarly, when the droplet volume is decreased the initial effect is that the contact angle decreases without motion of the contact line until the contact angle becomes less than a receding contact angle, θ_R. To set a droplet into motion the critical pinning force, F_c, that must be overcome is related to the difference in forces at the advancing and receding edges of the droplet, i.e.

$$F_c \sim 2\pi R \sin\theta \gamma_{LG}\left(\cos\theta_R - \cos\theta_A\right) \tag{1}$$

where the factor $2\pi R\sin\theta$ arises from the integration of forces around the droplet-solid contact line and R is the spherical radius of the droplet. The spherical radius of the droplet can be calculated from its volume, V,

$$R = \left[\frac{3}{\pi\left(2+\cos\theta\right)\left(1-\cos\theta\right)^2}\right]^{1/3} \tag{2}$$

To overcome the droplet transportation problem, one strategy is to use small-scale, micro- and/or nano-, surface texture or roughness to create a superhydrophobic surface to cause a droplet to ball-up with a large contact angle, θ, and small

droplet-solid contact line length (also referred to as the *Lotus* effect). In the ideal Cassie-Baxter state the droplet bridges between surface features as shown in Fig. 1(a) [31] and this has a small droplet footprint [8-12]. Moreover, the bridging between surface features also results in a high receding contact angle and, since $\theta_R<\theta<\theta_A$, the contact angle hysteresis is low and the droplet is highly mobile on the surface. However, this approach also reduces the area of droplet contact needed for an effective acoustic wave/liquid interaction. In addition, this Cassie-Baxter state itself can be unstable under a significant external perturbation such as SAW agitation, which can cause a rapid transition from a Cassie-Baxter state into a Wenzel state with the droplet penetrating between the surface features as shown in Fig. 1(b) [32]. In the Wenzel state, the droplet maintains complete contact with the surface features rather than bridging between them and the receding contact angle reduces substantially causing high values of contact angle hysteresis and low droplet mobility.

1.3.Slippery Liquid Infused Porous Surfaces (SLIPS)

An alternative approach to facilitating droplet transportation is to focus on reducing the contact angle hysteresis [22]. In the absence of contact angle hysteresis, contact line pinning is removed and a droplet will be highly mobile irrespective of its equilibrium contact angle and droplet-solid surface contact area [33, 34]. It is our hypothesis that reducing contact angle hysteresis and increasing droplet mobility without increasing the equilibrium contact angle towards 180^o could enable the twin objectives of ease of droplet actuation and large droplet contact area for acoustic wave interaction.

Recent advances in wetting research have seen the development of slippery liquid infused porous surfaces (SLIPS) inspired by the *Nepenthes Pitcher* plant. These

surfaces offer the high droplet mobility of superhydrophobic surfaces, whilst maintaining a large apparent droplet footprint (see Fig. 1(c)) [33]. The physical strategy is to create a large area surface texture using micro and/or nano-scale features which can be infused with a completely wetting non-volatile lubricating liquid, but which is hydrophobic to water thus preventing the lubricant being displaced. The high area surface texture means it is energetically favourable for the lubricant to spread into and be retained by the surface whilst also forming a stable thin film across the surface. In such a situation, a water droplet will rest on the lubricant layer, thus entirely removing direct contact between the droplet and the solid surface and the associated contact angle hysteresis which causes contact line pinning.

Smith *et al.* [35] has previously derived the absolute equilibrium thermodynamic states of a water droplet on a lubricant impregnated surface and described their relationship to the concept of hemi-wicking [36]. First consider a textured surface in air. The total interface energy per unit area for a lubricant oil to impregnate the surface and coat across the tops of surface features is $E_{(a)}=\gamma_{oa}+r_w\gamma_{os}$ where γ_{oa} and γ_{os} are the interfacial tensions (energies per unit area) of the oil-air and oil-solid interfaces. For this to be the lowest energy state possible, the spreading power of the oil on the solid in the presence of air, $S_{os(a)}$, must satisfy the condition,

$$S_{os(a)} = \gamma_{sa} - \left(\gamma_{os} + \gamma_{oa}\right) = \gamma_{oa}\left(\cos\theta_{os(a)} - 1\right) \geq 0 \qquad (3)$$

where $\theta_{os(a)}$ is the contact angle of oil on the solid in the presence of air. Thus, the equivalent condition is that the oil must completely wet the solid in air, i.e. $\theta_{os(a)}=0^o$, so that the oil is film forming on the solid in air.

Next consider the textured surface under water. The total interface energy per unit area for a lubricant oil to impregnate the surface and coat across the tops of surface features is $E_{(w)}=\gamma_{ow}+r_w\gamma_{os}$ where γ_{ow} is the interfacial tension (energy per unit area) of

the oil-water interface. For this to be the lowest energy state possible, the spreading power of the oil on the solid in the presence of water, $S_{os(w)}$, must satisfy the condition,

$$S_{os(w)} = \gamma_{sw} - (\gamma_{os} + \gamma_{ow}) = \gamma_{ow}(\cos\theta_{os(w)} - 1) \geq 0 \quad (4)$$

where $\theta_{os(w)}$ is the contact angle of oil on the solid in the presence of water. Thus, the equivalent condition is that the oil must completely wet the solid in water, i.e. $\theta_{os(w)}=0^{o}$, so that the oil is film forming on the solid in water.

In our previous work on droplet evaporation from SLIPS surfaces, we have observed that a droplet will inherently have a very low contact angle hysteresis [37] and be highly mobile, typically moving when a surface is tilted from the horizontal by less than 1^{o}, due to the existence of the lubricating layer. Ensuring conditions in eq. (3) and eq. (4) are satisfied, means that any motion of the droplet contact line always occurs on top of a lubricant film, which is retained by the solid surface in both air and water.

1.4. New design of SLIPS for SAW microfluidics

In the present work, we propose a new method for SAW-induced droplet actuation, which is built on our understanding of SLIP surfaces [22, 33, 34, 37, 38]. In our case the infused liquid is chosen to be a lubricant oil and by designing the SLIP surface layer to be significantly thinner than the SAW wavelength, we ensure that little damping of the acoustic wave occurs by the lubricant in the SLIP layer. The resulting surfaces support highly mobile droplets, whilst uniquely retaining the large footprint necessary for efficient dissipation of acoustic wave energy and momentum into the droplet. Furthermore, the lubricant impregnated surface structure ensures the droplet state is robust and less prone to the type of transition from a Cassie-Baxter state to a Wenzel state which can be observed on superhydophobic surfaces [11] due to

interaction with an acoustic wave. Our approach using the SLIPS enabled SAW droplet transportation offers low power actuation with a stable droplet state when a droplet is located within the SAW propagation path.

II. EXPERIMENTAL METHODS

To prove our concept and the key physical insight that slippery lubricant impregnated surfaces enable SAW-induced droplet transport due to their ability to also simultaneously maintain a large contact area, we coated SAW substrates with a thin self-assembled porous superhydrophobic layer infused with lubricating silicone oil (as illustrated in Figs. 2(a) to 2(c)). This surface treatment design provides a 3-D porous topography, with microscale and nanoscale features co-existing with hydrophobic nanoparticles, thus forming a superhydrophobic surface. Silicone oil spreads completely on these hydrophobic nanoparticles and into the porous structure in the presence of both air and water ($\theta_{os(a)} = 0^{\circ}$ and $\theta_{os(w)} = 0^{\circ}$) [39]. The lubricant oil impregnates and flows atop the surface features in air, but is also not displaced by the water in a deposited droplet (as shown in Figs. 2(b) and 2(c)). Thus, silicone oil impregnation converts the superhydrophobic surface into a SLIP surface. By controlling the roughness of the surface texture and the oil impregnation process, one can achieve the ideal case of a SLIP surface with high droplet mobility, but which also allows efficient SAW-induced droplet transportation.

ZnO films with a thickness of about 3.5 μm were deposited onto Si substrates using RF magnetron sputtering. Aluminium IDTs with a thickness of 150 nm were then fabricated using conventional lithographic and lift-off technology. The IDTs consisted of 30 pairs of fingers with a wavelength of 200 μm and an aperture of 4.9

mm. Rayleigh modes with a resonant frequency of 22.44 MHz with the same return loss were obtained for all the SAW devices.

The SAW device surfaces were treated using a commercially available water-repellent agent (Glaco^{TM} Mirror Coat "Zero", Soft 99 Co), which is an alcohol-based suspension of silica nanoparticles. The IDTs were covered by a Kapton tape during the coating process. The SAW devices were placed with a tilt angle of around 45° from the horizontal and then sprayed with the hydrophobic coating. The particle suspensions were left for 10 minutes to allow the solvent to evaporate. The device was then heated to 200 °C for 20 minutes. The process was repeated to produce SAW devices with between 1 and 5 coatings of the hydrophobic Glaco™ coating. Scanning electron microscopy (SEM) was used to characterise the surface morphology of the Glaco^{TM} coating on the ZnO/Si SAW devices. A Krüss DSA30 Contact Angle meter was used to measure advancing and receding contact angles to characterise the hydrophobic nature of the surfaces.

To create the SLIP surfaces, all the samples were dip-coated with silicone oil (Sigma-Aldrich, with a viscosity of 20 cSt (25℃) and a surface tension of 20.6 mNm^{-1}) by vertically withdrawing them from an oil reservoir at a speed of either 1 mm s^{-1} or 0.1 mm s^{-1}. We used the confocal laser scanning microscope to characterize the thickness of the oil. The thickness of the oil is proportional to the withdrawal speed and the measured thickness of the oil-layers for the two withdrawal speeds (1 mm s^{-1} or 0.1 mm s^{-1}) are 13.3±0.94 μm and 2.67 ±0.47 μm, respectively, which agreed well with the estimated values based on the reported work [39-41]. To characterize the droplet pinning on the surfaces of the SAW devices, sliding angle

measurements for water droplets on the SLIP surface of all the samples were carried out using the Krüss DSA30 Contact Angle meter equipped with a tilt stage. For a comparison of microfluidic performance, a CYTOP^{TM} layer (with a composition of 1,3,5,7-tetramethyl-2,4,8-trioxa-6-phenyl-6-phosphaadamantane) was used as an alternative surface coating of SAW devices. The spin coating process was used to coat CYTOP^{TM} (Asahi Glass Co., Ltd.) layer with a rotational speed of 2000 r/min. After baking at 100 ºC for 60 s, a CYTOP^{TM} layer with the thickness of 500 nm was obtained.

For the SAW droplet transportation experiments, the device IDTs were excited using an RF frequency of 22.44 MHz from a signal generator (Agilent Technologies, N9310A) with different powers, which were amplified using a broadband power amplifier (Amplifier Research, 75A250). The output power was measured using an RF power meter (Racal 9104). De-ionized (DI) water droplets of 2 μL were placed onto the SAW devices, 2 mm in front of the SAW IDTs. The movement of water droplets was recorded using a video camera. Droplet transport velocities were calculated from the recorded videos. Data on contact angles, tilt angles for sliding, threshold powers for droplet transportation (i.e. the minimum power required to initiate droplet motion) and velocity of droplet motion were determined from the average of three repeated tests.

Figures 3(a)-(c) show three typical SEM images of the ZnO/Si surfaces coated with 1, 2 and 4 Glaco^{TM} layers. Figure 3(a) is an image of a SAW device with a single coating of Glaco^{TM} and this suggests the surface has an evenly dispersed layer of silica nanoparticles. Figure 3(b) shows that the twice Glaco^{TM}-coated surface

possesses many stacked and accumulated silica nanoparticle structures making the surface increasingly rough and porous. Fig. 3(c) shows that the 4-fold coated Glaco^{TM}-coated surface possesses self-assembled clustered nanoparticle features and suggests that there are two scales of roughness and porosity: (1) a coarse scale of 0.5–2.0 μm composed of clusters or agglomerates of nanoparticles with average microscale holes of ~1 μm, and (b) nanoscale roughness that is characteristic of the size of the nanoparticles of around 40-50 nm together with nano-pores of ~50 nm. A combination of a microscale and nanoscale 3D porous morphology, and superhydrophobic properties was obtained through multiple coatings. Similar surface morphology has been reported by Vakarelski et. al. [41].

Figures 3(d)-(f) show 2 μL droplets of water are placed onto the surfaces. With increasing numbers of coated layers, the advancing and receding contact angles of the DI droplet increase as shown in Fig. 4. An advancing contact angle as large as ~170° is achieved for a 5-fold-coated surface together with a receding contact angle that indicates a low contact angle hysteresis, and thus demonstrates excellent superhydrophobic properties for the surface. Figure 4 also shows the static apparent contact angle of a 2 μL DI water on the SLIP surface created using an oil withdrawal speed of 0.1mm/s as a function of number of Glaco™ coatings. With increasing numbers of coated layers from 1-fold to 5 fold, the static apparent contact angle of a 2 μL DI water on SLIP surface increases from ~97° to ~109° before oil impregnation. The droplet pinning for each sample, after converting to a SLIP surface by infusion

with oil at a withdrawal speed of 0.1 mm/s, is illustrated by the tilt angle for sliding of water droplets in Fig. 4 as a function of number of coated layers. On the SLIP surface created using an oil withdrawal speed of 1 mm/s, the sliding angles at the same number of coated layers show similar values to those in the Fig. 4. With increasing number of the coated layers, the sliding angle decreases significantly below 1°.

From the SEM observations, it appears that the surfaces coated three-fold or more with the Glaco™ layer develop self-assembled porous structures, which become more evenly distributed on the surface with increasing the numbers of coatings. This type of structure may improve the retention of the lubricating oil on the surface, thus resulting in the progressive decrease of the sliding angle [40]. We believe that for four or more coatings, the surface may become saturated with the nanoparticles causing the sliding angle to saturate to a minimum. A sliding angle of 0.2° was observed on the 5-fold coated SLIP surface. The standard deviations of the sliding angles decrease with the increased numbers of coatings, indicating that the SLIP surfaces become uniform.

III. RESULTS AND DISCUSSION

The droplet transportation performance of the SAW devices with two coatings of the Glaco^{TM} suspension, with and without infusion with the lubricating oil, was investigated. Figures 5(a)-(e) show a 2 μL droplet on a surface not infused with oil (i.e., non-lubricated surface) before and after interaction with a SAW at an RF frequency of 22.44 MHz and an RF power of 2.5 W for various durations. Before applying the SAW power, the droplet shows a large contact angle (Fig. 5(a)). After applying the SAW power, the acoustic pressure applied to the droplet causes the droplet to deform into a conical shape whose trailing edge leans according to the Rayleigh angle as shown in Fig. 5(b). However, the droplet collapses quickly and the contact angle decreases significantly. In this case, the interaction with the SAW appears to cause the droplet to change from a Cassie-Baxter to a Wenzel state after applying with the RF SAW power, [12] i.e., the water penetrates into the surface features, thus reducing the contact angle significantly and converting the surface into one with large contact angle hysteresis and droplet pinning. The droplet was observed to vibrate significantly, but without any movement as shown in Figs. 5(b)-(d) because of the large contact angle hysteresis of the Wenzel state. When the SAW power was turned off, the contact angle was observed to have been reduced to ~ 60° (see Fig. 5(e)).

Figures 5(f)-(j) show the effect of SAW interaction with a 2 μL droplet on a similar surface, but infused with silicone oil created using an oil withdrawal speed of

0.1 mm/s. Before applying an RF SAW power of 2.5 W, the droplet shows a large footprint on the SLIP surface (see Fig. 5(f)) because of the silicone oil infused into the surface. After applying the SAW power, the apparent contact angle remains almost a constant and the droplet moves smoothly across the surface as shown in Figs. 5(g)-(i). By using the Glaco^{TM}-coating, the surface of SAW devices has a combined micro-roughness structures and nanoscale-roughness structures which make it superhydrophobic with a large contact angle (see Fig. 3(f)) and this porous structure then facilitates the retention of the lubricating oil on the surface. The droplet has a low surface friction when moving on the oil infused surface and it therefore slides easily [36, 39, 42, 43]. Moreover, the SLIP surface provides a sufficiently large footprint (see Figs. 1(c), 2(b) and 5(f)-(j)), to facilitate the transfer of SAW energy into the droplet, enhancing its transportation efficiency. When the SAW power was turned off, the apparent contact angle (~ 110^{o}) was similar to that before the SAW power was applied (see Figs. 5(f) and (j)).

The SAW microfluidics performance of a 2 μL DI water on the SLIP surfaces treated with different numbers of coated layers and silicone oil layer thickness was investigated. As seen from Fig. 6(a), the threshold power required to move a droplet decreases with increasing number of coated layers. With increasing numbers of coated layers, the contact angle θ of the non-oil infused SAW surface increases (Fig. 4). Moreover, because of the decrease in the sliding angle and the existence of a large droplet footprint on the SLIP surface, the threshold powers for the droplet

transportation decrease with the increase in the number of coated layers. A power as low as 0.9 W was capable of driving the droplet motion on the SAW devices treated with five Glaco™ layers and an oil withdrawal speed of 0.1 mm/s. In comparison, the threshold power to move a droplet with the same droplet volume on a standard CYTOP™-coated SAW device was found to be 6 W. Therefore, the threshold power of droplet transportation for the SLIP surface SAW devices treated with 5-fold coated Glaco™ layers and the oil withdrawal speed of 0.1 mm/s was reduced over 85% compared to CYTOP™-coated SAW devices.

As shown in Fig. 6(a), the threshold power to initiate droplet motion for the SLIP SAW device with the oil withdrawal speed of 0.1 mm/s is much smaller than that of SLIP surface with the oil withdrawal speed of 1 mm/s for the same number of coated layers. According to the literature, the faster the withdrawal speed, the thicker the layer [36, 40, 43,]. Therefore, the results in Fig. 6(a) are consistent with expectations as the SAW vibration and energy should be damped by increasingly thick layers of oil.

Figure 6(b) shows the velocity of a 2 μL DI water droplet moving on the SLIP surface actuated using an RF power of 7 W as a function of the number of Glaco™ coatings. The droplet velocity increases as the number of coats increases. A velocity of more than 38 mm/s is observed on a SLIP surface coated with five layers of Glaco™ and an oil withdrawal speed of 0.1 mm/s, which is more than 14 times larger

than that of a single layer coated SLIP surface with the same oil thickness. With the increase in the number of coatings, the surface friction decreases and the threshold power for droplet motion decreases, therefore, at the same power, the droplet velocity increases dramatically. The droplet velocity for the SLIP surface with the oil withdrawal speed of 0.1 mm/s is much larger than that of the SLIP surface with the oil withdrawal speed of 1 mm/s and the same number of Glaco™ coats due to the decreased attenuation of the SAW with the thinner oil layer on the SLIP surface.

We tested the SAW microfluidics performance on the same devices more than 100 times. The results showed almost the same phenomena without increase of the threshold power for droplet transportation or decrease of the droplet velocity. Furthermore, we left the devices in air without protection and tested their SAW microfluidics performance frequently after more than three weeks. The threshold powers for droplet transportation and the droplet velocity remained nearly the same values. Results showed that the SLIP surface is robust and that the SAW microfluidics on SLIP surface show good repeatability and long-term stability.

IV. CONCLUSION

In brief, a new strategy to reduce droplet contact line pinning and enable SAW induced droplet transportation has been developed. By creating ZnO/Si SAW devices with a SLIP surface achieved by infusing a superhydrophobic porous nanoparticulate surface with a lubricating oil, efficient droplet movement with significant reductions

in the threshold power and higher droplet velocities were achieved. In this approach, the contact angle hysteresis is reduced to overcome contact line pinning, whilst retaining a sufficiently large droplet footprint to facilitate SAW energy to be dissipated into the droplet. To enable the SLIP surface coating approach to be combined with effective propagation of SAWs on the device surfaces without large acoustic wave attenuation the oil layer due to the SLIP surface has to be designed to be much thinner than the SAW wavelength. The SLIP surfaces on SAW devices presented in this work are easy to fabricate, inexpensive and reproducible, which is promising for droplet microfluidics based on SAWs.

ACKNOWLEDGMENTS

The authors' acknowledge financial support from NSFC (Grant no. 51302173), National Key Research and Development Program of China (Grant no. 2016YFB0402705), Basic Research Program of Shenzhen (Grant no. JCYJ20140418091413493), and Royal Academy of Engineering: Research Exchange between UK and China was acknowledged. We would also like to thank the UK Engineering and Physical Sciences Research Council (EPSRC) for support under grant EP/L026899/1 and EP/P018998/1 and Knowledge Transfer Partnership No KTP010548.

Figure Captions:

Figure 1 Three states of surface wetting influenced by topography. (a) The Cassie–Baxter state involves the droplet bridging between the tips of surface features thus reducing solid-liquid interfacial area. The droplet has a small footprint and high mobility. (b) The Wenzel state involves the droplet penetrating between surface features thus increasing the solid-liquid interfacial area. The droplet sticks to the surface and has low mobility. (c) The lubricant impregnated surface retains lubricant due to it wetting a high surface area nanoparticle porous structure whose hydrophobic properties ensure the lubricant is not displaced by water. The droplet has a large footprint and high mobility.

Figure 2 (a) Schematic illustration of a SAW device with a SLIP surface; (b) Schematic illustration of the interaction between a SAW and a liquid droplet on a SLIP surface. The Rayleigh angle θ_R and a larger droplet footprint enabling effective transfer of SAW energy to drive the droplet motion are indicated; (c) Illustration of enlarged interface between the droplet and the lubricant oil.

Figure 3 SEM images of hydrophobic silica nanoparticle surfaces created using different numbers of Glaco coatings: (a) single coating, (b) double coating, and (c) four-fold coating. Insets are the larger magnification SEM images. (d)-(f) the corresponding images for a 2 μL droplet of water on each of the above surfaces.

Figure 4 Left-hand Y-axis shows the sliding angles (i.e., angles of substrate tilt needed to initiate droplet sliding) of a 2μL DI water on SLIP surface created using an

oil withdrawal speed of 0.1mm/s as a function of number of Glaco™ coatings. Right-hand Y-axis shows the advancing and receding contact angles of a 2μL DI water on the surface before oil impregnation as a function of number of Glaco™ coatings and also shows the apparent contact angle of a 2μL DI water on SLIP surface created using an oil withdrawal speed of 0.1mm/s as a function of number of Glaco™ coatings.

Figure 5 The SAW microfluidic performance of a 2μL DI water droplet on SAW devices with double Glaco ・ coatings and an applied SAW power of 2.5 W at a frequency of 22.44 MHz after various durations. (a)-(e) shows the SAW device without silicone oil. (a) before applied SAW power, (b) applied SAW power 0.05 s, (c) 0.12 s, (d) 0.19 s and (e) after turning off the SAW power. (f)-(j) shows the SAW device impregnated with silicone oil and the oil treatment of 0.1 mm/s. (f) before applied SAW power, (g) applied SAW power 0.05s, (h) 0.12s (i) 0.19s (j) after turning off the SAW power.

Figure 6 (a) The threshold powers for droplet transportation of a 2μL DI water using a frequency of 22.44 MHz RF signal for surfaces created with two oil withdrawal speeds depending on the number of Glaco ・ coatings; (b) droplet velocity of a 2μL DI water on SAW devices using a RF power of 7W at the frequency of 22.44 MHz as a function of number of coatings.

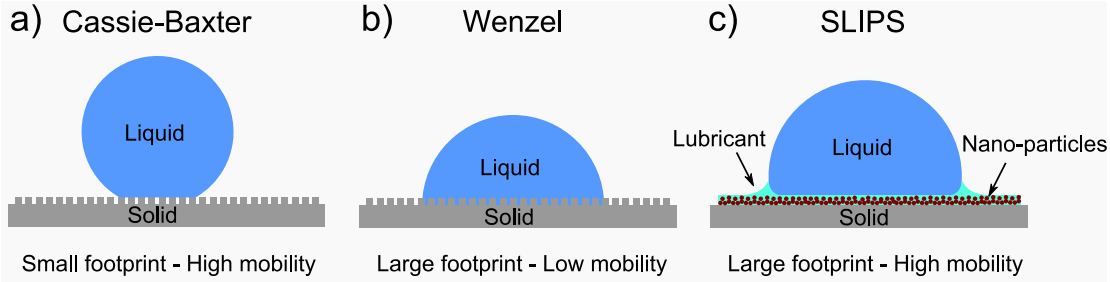
a) Cassie-Baxter
Liquid
Solid
Small footprint - High mobility
b) Wenzel
Liquid
Solid
Large footprint - Low mobility
c) SLIPS
Lubricant
Liquid
Nano-particles
Solid
Large footprint - High mobility

Fig. 1

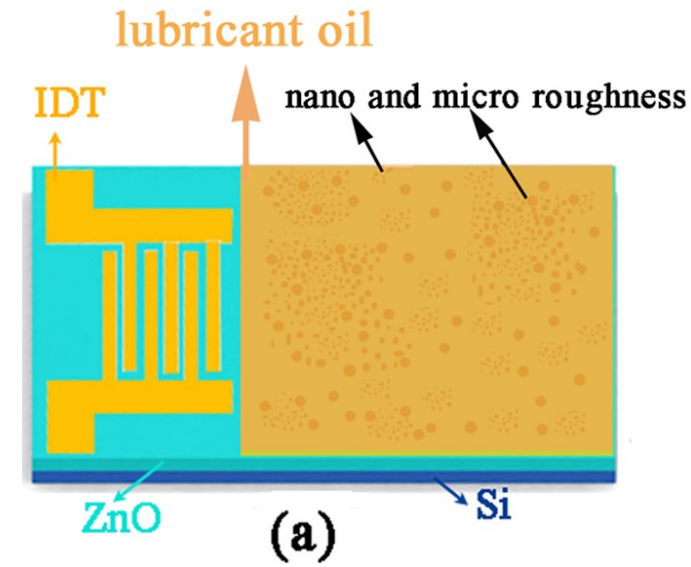
lubricant oil
IDT
nano and micro roughness
ZnO
Si
(a)

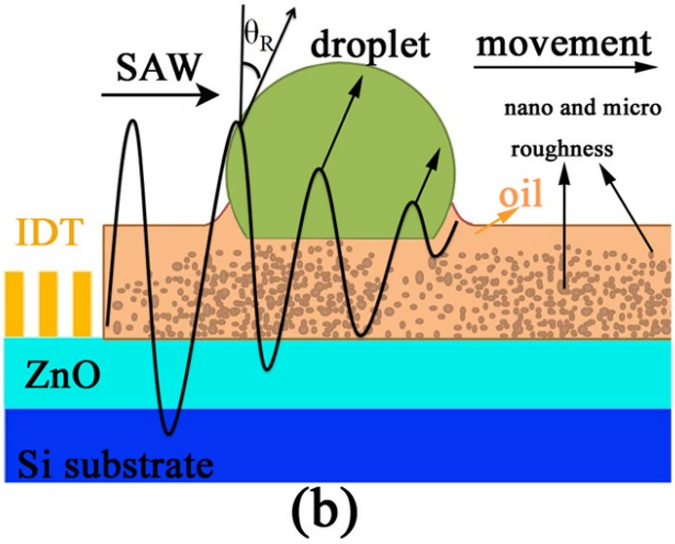
θR
droplet
movement
SAW
nano and micro
roughness
oil
IDT
ZnO
Si substrate
(b)

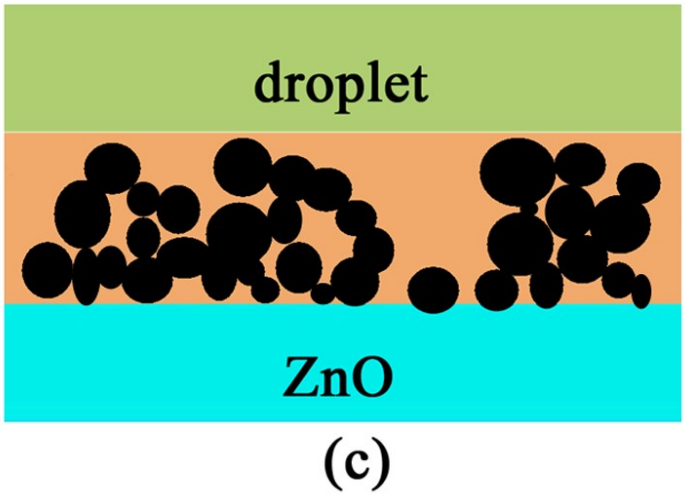
droplet
ZnO
(c)

Fig. 2

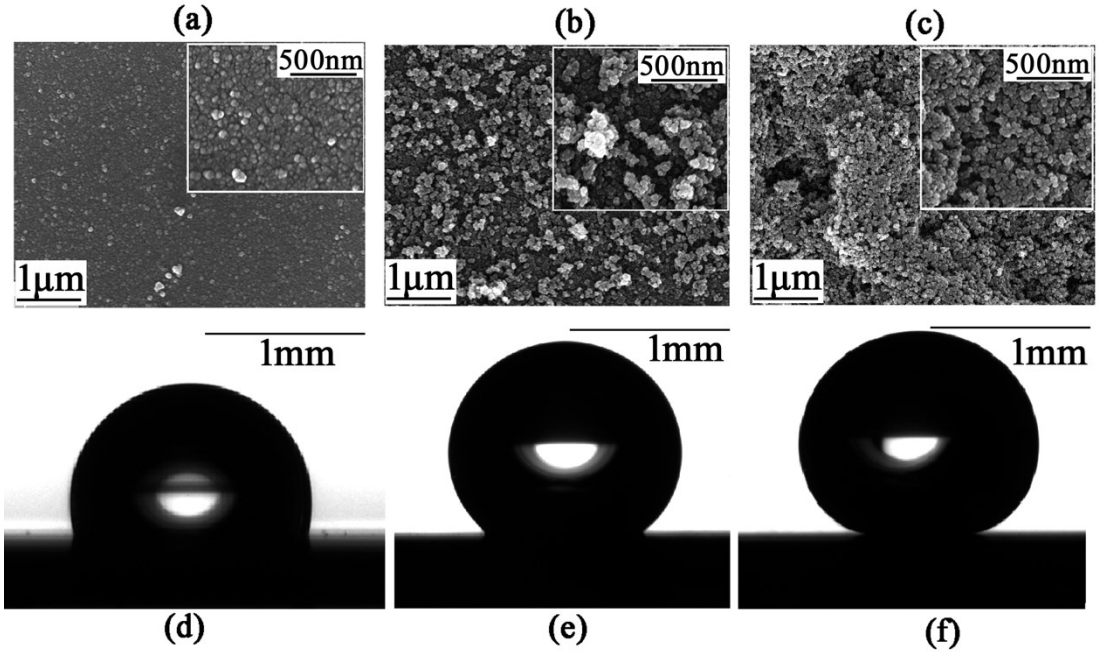
(a)
(b)
(c)
500nm
500nm
500nm
1μm
1μm
1μm
1mm
1mm
1mm
(d)
(e)
(f)

Fig. 3

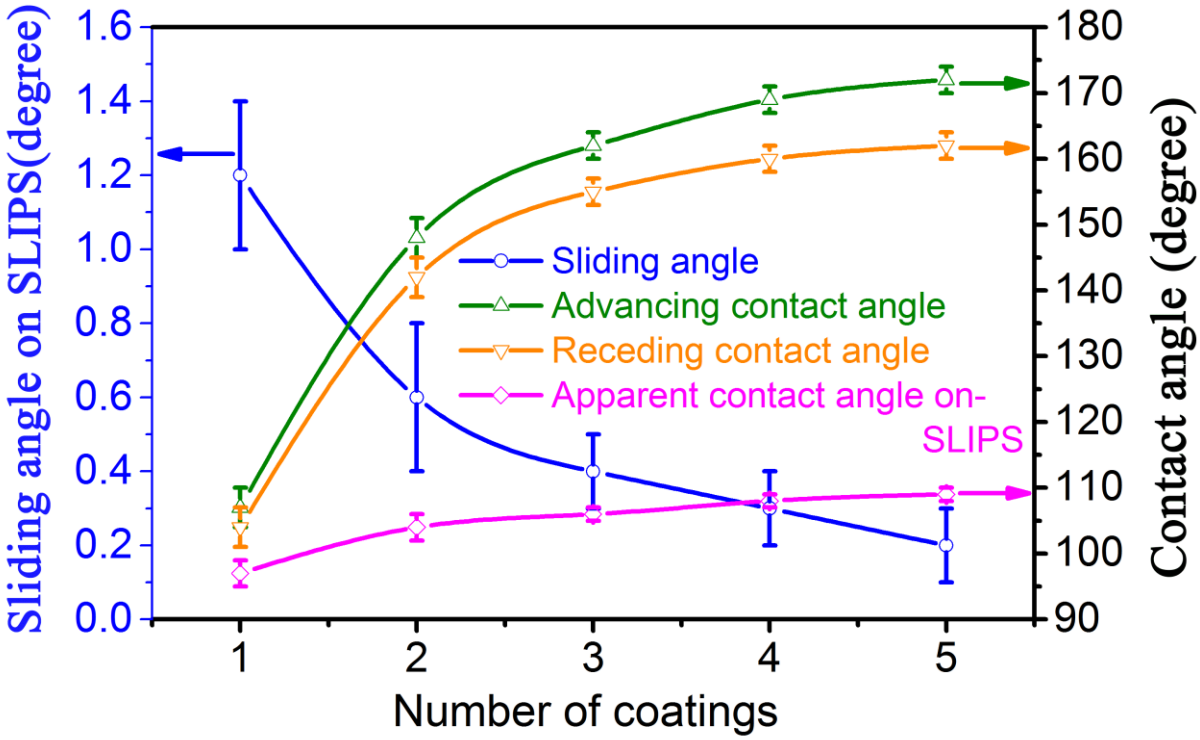
Sliding angle on SLIPS(degree)
Contact angle (degree)
Number of coatings
Sliding angle
Advancing contact angle
Receding contact angle
Apparent contact angle on-SLIPS
0.0
0.2
0.4
0.6
0.8
1.0
1.2
1.4
1.6
90
100
110
120
130
140
150
160
170
180
1
2
3
4
5

Fig. 4

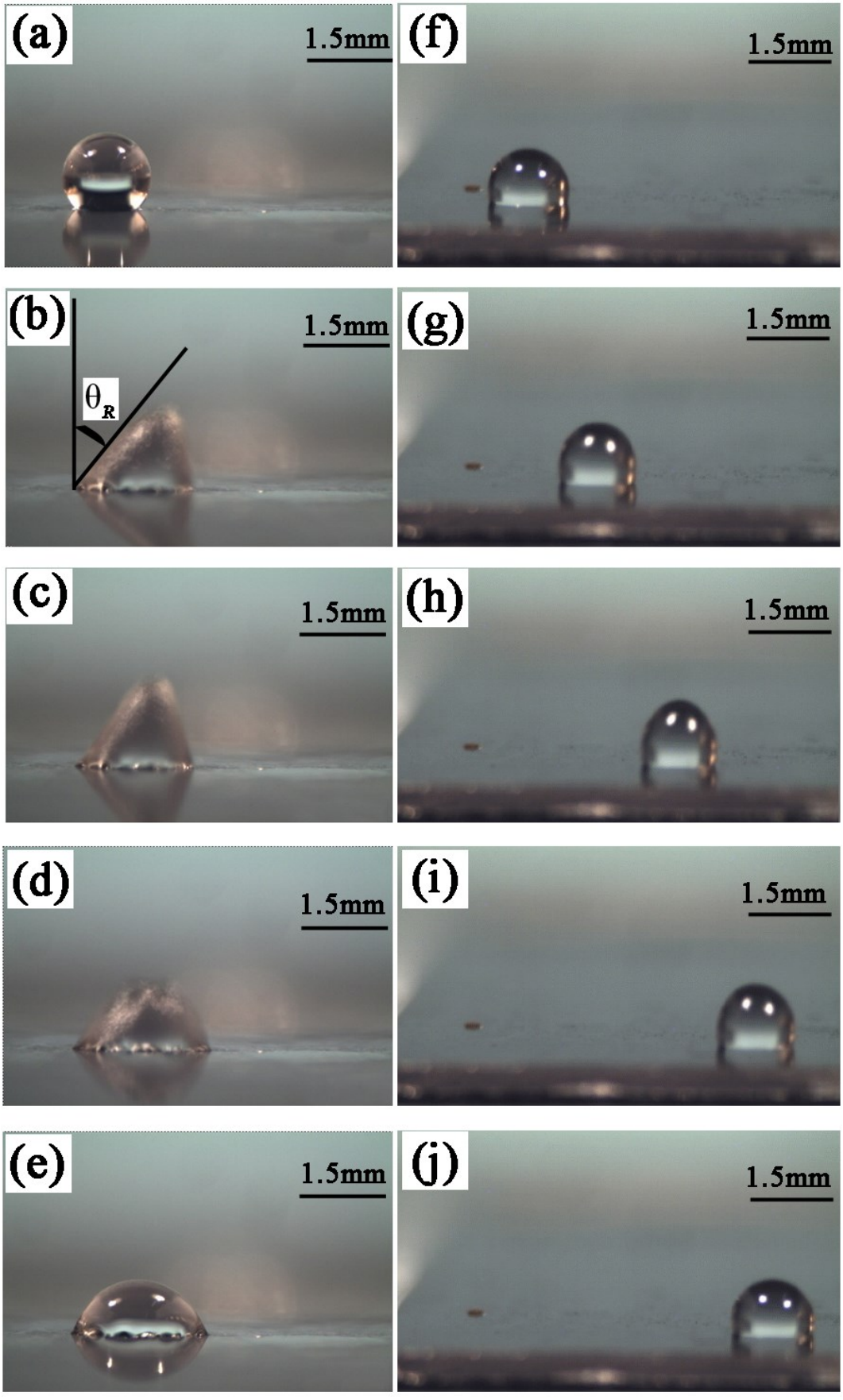
(a)
1.5mm
(f)
1.5mm
(b)
1.5mm
θR
(g)
1.5mm
(c)
1.5mm
(h)
1.5mm
(d)
1.5mm
(i)
1.5mm
(e)
1.5mm
(j)
1.5mm

Fig. 5

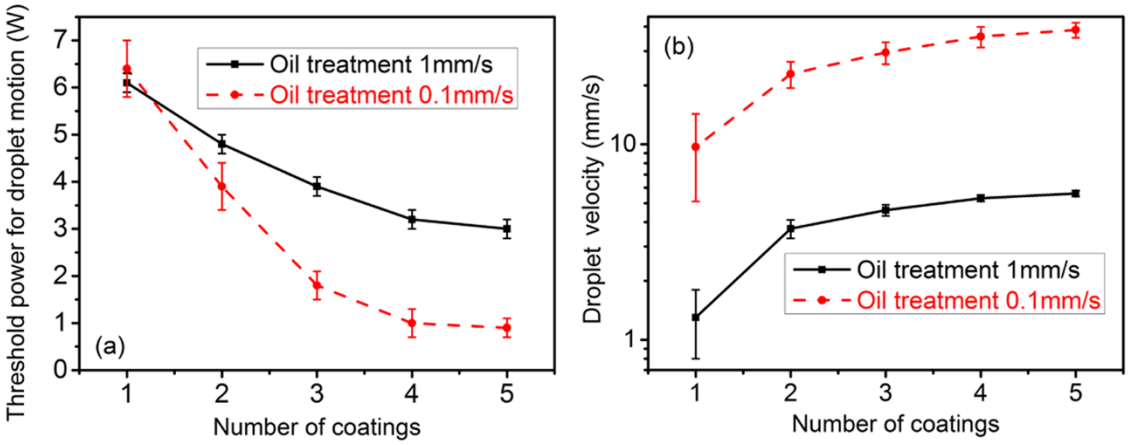
Threshold power for droplet motion (W)
Oil treatment 1mm/s
Oil treatment 0.1mm/s
(a)
Number of coatings
Droplet velocity (mm/s)
(b)
Oil treatment 1mm/s
Oil treatment 0.1mm/s
Number of coatings

Fig. 6

REFERENCES

[1] P. de Gennes, *Wetting: statics and dynamics*, Rev. Mod. Phys. **57**, 827 (1985).

[2] J. Joanny, and P. de Gennes, *A model for contact angle hysteresis*, J. Chem. Phys. **81**, 552 (1984).

[3] A. W. Adamson, and A. P. Gast, *Physical Chemistry of Surfaces*, Wiley-Blackwell; 6th Ed. (1997) ISBN-10: 0471148733.

[4] R. D. Deegan, O. Bakajin, T. F. Dupont, G. Huber, S. R. Nagel, and T. A. Witten, *Capillary flow as the cause of ring stains from dried liquid drops*, Nature **389**, 827 (1997).

[5] G. McHale, *Surface free energy and microarray deposition technology*, Analyst **132**, 192 (2007).

[6] M. Singh, H. M. Haverinen, P. Dhagat, and G. E. Jabbour, *Inkjet printing-process and its applications*, Adv. Maters **22**, 673 (2010).

[7] S. Y Teh, R. Lin, L. H Hung, and A. P. Lee, *Droplet microfluidics*, Lab Chip **8**, 198 (2008).

[8] T. Onda, S. Shibuichi, N. Satoh, and K. Tsujii, *Super-water-repellent fractal surfaces*, Langmuir **12**, 2125 (1996).

[9] W. Barthlott, and C. Neinhuis, *Purity of the sacred lotus, or escape from contamination in biological surfaces*, Planta **202**, 1 (1997).

[10] C. Neinhuis, C., and W. Barthlott, *Characterization and distribution of water-repellent, self-cleaning plant surfaces*, *Ann. Botan.* **79**, 667 (1997).

[11] D. Quéré, *Wetting and roughness*, Annu. Rev.Mater. Res. **38**, 71 (2008).

[12] N. J. Shirtcliffe, G. McHale, S. Atheron, and M. I. Newton, *An introduction to superhydrophobicity*, Adv Colloid Interface Sci. **161**, 124 (2010).

[13] L. Y. Yeo and J. R. Friend, *Ultrafast microfluidics using surface acoustic waves*, Biomicrofluidics **3**, 012002 (2009).

[14] Y. Q. Fu, J. K. Luo, X. Y. Du, A. J. Flewitt, Y. Li, G. H. Markx, A. J. Walton, and W. I. Mine, *Recent developments on ZnO films for acoustic wave based bio-sensing and microfluidic applications: a review*, Sensor. Actuat. B-Chem. **143**, 606 (2010).

[15] X. Ding, P. Li, S. C. S. Lin, Z. S. Stratton, N. Nama, F. Guo, D. Slotcavage, X. L. Mao, J. J. Shi, and F. Costanzo, *Surface acoustic wave microfluidics*, Lab Chip **13**, 3626 (2013).

[16] J. T. Luo, M. Xie, P. X. Luo, B. X. Zhao, K. Du and F. Pan, *A sensitive glucose biosensor without using glucose test strips based on ZnO/SiO_2/Si surface acoustic wave device*, Mater. Lett. **130**, 14 (2014).

[17] L. Y. Yeo and J. R. Friend, *Surface acoustic wave microfluidics*, Annu. Rev. Fluid. Mech. **46**, 379 (2014).

[18] J. T. Luo, P. X. Luo, M. Xie, K. Du, B. X. Zhao, F. Pan, P. Fan, F. Zeng, D. P. Zhang, Z. H. Zheng, and G. X. Liang, *A new type of glucose biosensor based on surface acoustic wave resonator using Mn-doped ZnO multilayer structure*, Biosens. Bioelectron. **49**, 512 (2013).

[19] J. J. Xu, Z. J. Lei, J. K. Guo, J. Huang, W. Wang, U. Reibetanz, and S. Y. Xu, *Trapping and driving individual charged micro-particles in fluid with an electrostatic device*, Nano-Micro Lett. **8**, 270 (2016).

[20] A. Barani, H. Paktinat, M. Janmaleki, A. Mohammadi, P. Mosaddegh, A. Fadaei-Tehrani, and A. Sanati-Nezhad, *Microfluidic integrated acoustic waving for manipulation of cells and molecule*s, Biosens. Bioelectron. **85**, 714 (2016)

[21] M. C. DeSantis and W. Cheng, *Label-free detection and manipulation of single biological nanoparticles*, WIREs Nanomed. Nanobiotechnol. **8**, 717 (2016)

[22] T. S. Wong , T. Sun, L. Feng, and J. Aizenberg, *Interfacial materials with special wettability*, MRS Bulletin, **38** 366 (2013).

[23] Z. Wang, M. Elimelech, and S. Lin, *Environmental applications of interfacial materials with special wettability*, Environ. Sci. & Technol. **50**, 2132 (2016).

[24] H. Chen, T. Tang, H. Zhao, K. Y. Law, and A. Amirfazli, *How pinning and contact angle hysteresis govern quasi-static liquid drop transfer*. Soft Matter **12**,1998 (2016).

[25] J. Yang, and D. Y. Kwok, *Analytical treatment of electrokinetic microfluidics in hydrophobic microchannels*, Anal. Chim. Acta **507**, 39 (2004).

[26] J. K. Luo, Y. Q. Fu, Y. Li, X. Y. Du, A. J. Flewitt, A. J. Walton, and W. I. Milne, *Moving-part-free microfluidic systems for lab-on-a-chip*, J. Micromech. Microeng. **19**, 054001 (2009).

[27] X. Y. Du, M. E. Swanwick, Y. Q. Fu, J. K. Luo, A. J. Flewitt, D. S. Lee, S. Maeng, and W. I. Milne, *Surface acoustic wave induced streaming and pumping in 128 Y-cut $LiNbO_3$ for microfluidic applications*, J. Micromech. Microeng. **19**, 035016 (2009).

[28] S. Girardo, M. Cecchini, F. Beltram, R. Cingolani, and D. Pisignano, *Polydimethylsiloxane–$LiNbO_3$ surface acoustic wave micropump devices for fluid control into microchannels*, Lab Chip **8**, 1557 (2008).

[29] X. Y. Du, Y. Q. Fu, J. K. Luo, A. J. Flewitt, and W. I. Milne, *Microfluidic pumps employing surface acoustic waves generated in ZnO thin films***,** J. Appl. Phys. **105**, 024508 (2009).

[30] Y. Liu, Y. F. Li, A. M. el-Hady, C. Zhao, J. F. Du, Y. Liu, and Y. Q. Fu, *Flexible and bendable acoustofluidics based on ZnO film coated aluminium foil*, Sensor. Actuat. B-Chem. **221**, 230 (2015).

[31] A. B. D Cassie, and S. Baxter, *Wettability of Porous Surfaces*, Trans. Faraday Soc. **40**, 546 (1944).

[32] R. N. Wenzel, *Resistance of Solid Surfaces to Wetting by Water*. Ind. Eng. Chem. **28**, 988 (1936).

[33] T.-S. Wong, S. H. Wong, S. K. Y. Tang, E. J. Smythe, B. D. Hatton, A. Grinthal, and J. Aizenberg, *Bioinspired self-repairing slippery surfaces with pressure-stable omniphobicity*, Nature **477**, 443 (2011).

[34] M. Nosonovsky, Materials science: Slippery when wetted, Nature **477**, 412 (2011).

[35] J. D. Smith, R. Dhiman, S. Anand, E. Reza-Garduno, R. E. Cohen, G. H. McKinley, and K. K. Varanasi, *Droplet mobility on lubricant-impregnated surfaces*, Soft Matter **9**, 1772 (2013).

[36] J. Bico, U. Thiele, and D. Quere, *Wetting of Textured Surfaces*. Colloids Surf., A **206**, 41 (2002).

[37] J. H. Guan, G. G. Wells, B. Xu, G. McHale, D. Wood, J. Martin and S. Stuart-Cole, *Evaporation of sessile droplets on slippery liquid-infused porous surfaces (SLIPS)*, Langmuir **31**, 11781 (2015).

[38] C. Semprebon, G. McHale, and H. Kusumaatmaja, *Apparent contact angle and contact angle hysteresis on liquid infused surfaces*, Soft Matter, Advance Article (2016). DOI: 10.1039/C6SM00920D.

[39] B.R. Solomon, K.S. Khalil, and K.K. Varanasi, *Drag reduction using lubricant-impregnated surfaces in viscous laminar flow*, Langmuir **30**, 10970 (2014).

[40] J. C. Seiwert, C. Clanet, and D. Quéré, *Coating of a textured solid*, J. Fluid Mech. **669**, 55 (2011).

[41] I.U. Vakarelski, N. A. Patankar, J. O. Marston, D. Y. C. Chan, S. T. Thoroddsen, *Stabilization of Leidenfrost vapour layer by textured superhydrophobic surfaces*, Nature **489**, 274 (2012).

[42] X. Huang, J. D. Chrisman, and N. S. Zacharia, *Omniphobic slippery coatings based on lubricant-infused porous polyelectrolyte multilayers*, ACS Macro Lett. **2**, 826 (2013).

[43] F. Schellenberger, J. Xie, N. Encinas, A. Hardy, M. Klapper, P. Papadopoulos, H. J. Butt, and D. Vollmer, *Direct observation of drops on slippery lubricant-infused surfaces*, Soft Matter **11**, 7617 (2015).\